J. Fluid Mech. (2010), *vol.* 656, *pp.* 177–188. © Cambridge University Press 2010
doi:10.1017/S0022112010001473

Structure of a steady drain-hole vortex in a viscous fluid

L. BØHLING[1,2], A. ANDERSEN[1]† AND D. FABRE[3]

[1]Department of Physics and Center for Fluid Dynamics, Technical University of Denmark, DK-2800 Kgs. Lyngby, Denmark

[2]Niels Bohr Institute, Blegdamsvej 17, DK-2100 Copenhagen Ø, Denmark

[3]Université de Toulouse, INPT, UPS; Institut de Mécanique des Fluides de Toulouse (IMFT), Allée du Professeur Camille Soula, F-31400, Toulouse, France

(Received 15 October 2009; revised 19 March 2010; accepted 19 March 2010; first published online 10 June 2010)

We use direct numerical simulations to study a steady bathtub vortex in a cylindrical tank with a central drain-hole, a flat stress-free surface and velocity prescribed at the inlet. We find that the qualitative structure of the meridional flow does not depend on the radial Reynolds number, whereas we observe a weak overall rotation at a low radial Reynolds number and a concentrated vortex above the drain-hole at a high radial Reynolds number. We introduce a simple analytically integrable model that shows the same qualitative dependence on the radial Reynolds number as the simulations and compares favourably with the results for the radial velocity and the azimuthal velocity at the surface. Finally, we describe the height dependence of the radius of the vortex core and the maximum of the azimuthal velocity at a high radial Reynolds number, and we show that the data on the radius of the vortex core and the maximum of the azimuthal velocity as functions of height collapse on single curves by appropriate scaling.

1. Introduction

Concentrated vortex flows range from small laboratory whirlpools to large atmospheric tornadoes (Lugt 1995). Bathtub vortex flows constitute an important class of concentrated vortex flows which are characterized by intense axial down-flow and stress-free surface. Such flows typically form at intake pipes and tank outlets, and they have been studied with focus on different intriguing aspects. Shapiro (1962) and Trefethen *et al.* (1965) investigated the influence of the Coriolis force on the sense of rotation, Andersen *et al.* (2003) found a needle-like tip structure in a steady bathtub vortex with strong rotation, Tyvand & Haugen (2005) considered the time evolution of a bathtub vortex formed because of an impulsive sink, and Stepanyants & Yeoh (2008*b*) modelled the rate of discharge at which the surface depression reaches the outlet.

In this study, we use direct numerical simulations to explore the flow structure of a steady bathtub vortex in an incompressible Newtonian fluid. We assume that the flow has rotational symmetry and we simulate the source-sink flow in a cylindrical tank with a central drain-hole and a flat stress-free surface. At the inlet, we prescribe

† Email address for correspondence: aanders@fysik.dtu.dk

https://doi.org/10.1017/S0022112010001473 Published online by Cambridge University Press

the radial and azimuthal velocities and thereby control both the radial Reynolds number and the azimuthal Reynolds number. The simulations demonstrate a weak overall rotation at a low radial Reynolds number and a concentrated vortex above the drain-hole at a high radial Reynolds number. The simulations also show that the flow structure has little dependence on the azimuthal Reynolds number. The transition from a weak overall rotation to a concentrated vortex takes place at parameter values at which the assumption of a flat stress-free surface is applicable in typical laboratory situations. It is well known that the radius of the core of a viscous bathtub vortex results from the balance between the outward transport of vorticity due to viscous diffusion and the inward advective transport of vorticity and the axial vortex stretching (Batchelor 1967; Guyon *et al.* 2001; Alekseenko, Kuibin & Okulov 2007). An instructive example is provided by the Burgers vortex, which was first considered by Burgers (1940) and has later been used as a bathtub vortex model by Rott (1958), Miles (1998) and Stepanyants & Yeoh (2008*a*). The meridional flow in the Burgers vortex describes the flow near a stagnation point well, but it does not allow for modelling of two features which are potentially important in bathtub vortex flows. First, the axial velocity in the Burgers vortex does not depend on the distance to the vortex axis, and second the axial vortex stretching does not vary along the vortex axis (Rossi *et al.* 2004). The first point, which is important for modelling the overall vortex structure, is addressed in the approximate model by Einstein & Li (1951), in which an inner Burgers vortex and an outer rotational flow without down-flow are matched. The Einstein and Li model was discussed by Lewellen (1962) and shown to be an applicable approximation of the Navier–Stokes equations when the ratio of sink flow to circulation is small. In the following we introduce an integrable model with a smooth axial velocity profile that belongs to the same general class of vortex models. We show that the approximate model describes the surface flow well and captures the dependence on the radial Reynolds number. In relation to the second point, we describe the height dependence of the radius of the vortex core and the maximum of the azimuthal velocity at high radial Reynolds number. Finally, we discuss a possible experimental realization of the flow and evaluate our results in relation to vortex formation through spontaneous symmetry breaking.

2. Direct numerical simulations

2.1. *Geometry and control parameters*

We consider a steady source-sink flow with rotational symmetry in a cylindrical tank with a central drain-hole as sketched in figure 1(*a*). Fluid enters the tank horizontally with specified velocity at the outer cylindrical boundary and leaves the tank through the circular drain-pipe at the centre of the bottom. We denote the radius of the tank R, the height of the tank H, the radius of the drain-pipe R_d and the height of the drain-pipe H_d. We use cylindrical polar coordinates (r, ϕ, z) with $z = 0$ coinciding with the bottom of the tank and denote the velocity components (v_r, v_ϕ, v_z). The source-sink flow is characterized by the volume flow rate Q and it is convenient to define the radial flow rate per unit height $q = Q/H$. The corresponding radial Reynolds number based on the tank radius and the average radial velocity at the inlet is $Re_r = -R\,\overline{V}_r/\nu = q/(2\pi\nu)$, where ν is the kinematic viscosity. The azimuthal Reynolds number based on the tank radius and the average azimuthal velocity at the inlet is $Re_\phi = R\,\overline{V}_\phi/\nu$.

https://doi.org/10.1017/S0022112010001473 Published online by Cambridge University Press

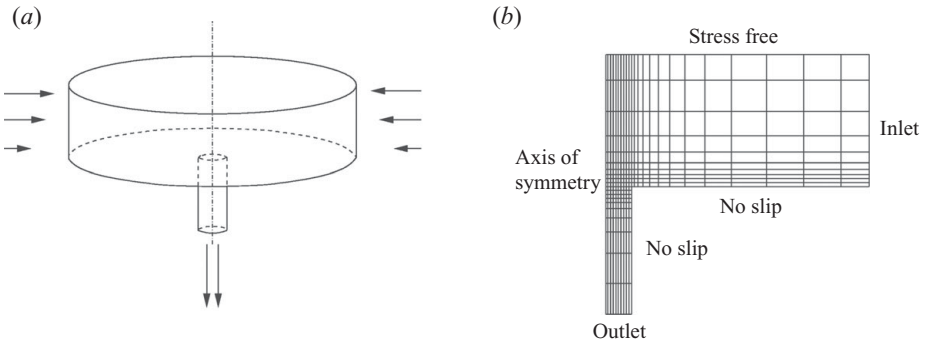


FIGURE 1. (*a*) Sketch of the three-dimensional cylindrical tank with the inlet at the outer rim and the drain-hole at the centre of the bottom. (*b*) The two-dimensional computational domain. For clarity we only show every third horizontal line and every second vertical line in the mesh used for the simulations with $H/R = 0.50$ at a low radial Reynolds number.

2.2. *Method*

The simulations were performed using the code JADIM, which is currently developed and used for a variety of problems at Institut de Mécanique des Fluides de Toulouse (Magnaudet, Rivero & Fabre 1995; Auguste, Fabre & Magnaudet 2010). Here the code solves the equation of continuity

$$\frac{\partial v_r}{\partial r} + \frac{v_r}{r} + \frac{\partial v_z}{\partial z} = 0, \tag{2.1}$$

and the incompressible Navier–Stokes equations

$$v_r \frac{\partial v_r}{\partial r} + v_z \frac{\partial v_r}{\partial z} - \frac{v_\phi^2}{r} = -\frac{1}{\rho}\frac{\partial p}{\partial r} + \nu\left(\frac{\partial^2 v_r}{\partial r^2} + \frac{1}{r}\frac{\partial v_r}{\partial r} - \frac{v_r}{r^2} + \frac{\partial^2 v_r}{\partial z^2}\right), \tag{2.2}$$

$$v_r \frac{\partial v_\phi}{\partial r} + v_z \frac{\partial v_\phi}{\partial z} + \frac{v_r v_\phi}{r} = \nu\left(\frac{\partial^2 v_\phi}{\partial r^2} + \frac{1}{r}\frac{\partial v_\phi}{\partial r} - \frac{v_\phi}{r^2} + \frac{\partial^2 v_\phi}{\partial z^2}\right), \tag{2.3}$$

$$v_r \frac{\partial v_z}{\partial r} + v_z \frac{\partial v_z}{\partial z} = -\frac{1}{\rho}\frac{\partial p}{\partial z} + \nu\left(\frac{\partial^2 v_z}{\partial r^2} + \frac{1}{r}\frac{\partial v_z}{\partial r} + \frac{\partial^2 v_z}{\partial z^2}\right), \tag{2.4}$$

where ρ is the density and p is the pressure. The code uses a finite-volume method on a Cartesian mesh in the meridional plane as shown in figure 1(*b*). The mesh is non-uniform and refined in the vicinity of the inlet of the drain-pipe where the gradients are largest. We apply a no-slip boundary condition at the bottom of the tank and at the surface of the central drain-pipe. The free surface is approximated as flat and a stress-free boundary condition is applied on it. This approximation is valid whenever the Froude number is small (De Felice 2007). We define the Froude number $Fr = V^2/(g\,H)$, where V is the magnitude of the characteristic velocity at the surface and g is the acceleration due to gravity (Landau & Lifshitz 1987). Defined in this way, the Froude number is for a fluid particle at the surface an estimate of the ratio of its kinetic energy and its gravitational potential energy relative to the bottom, and the Froude number is therefore a measure of the magnitude of the surface deformation relative to the height of the tank. The approximation is, in other words, valid when the magnitude of the velocity at the surface is small in comparison with the outflow velocity for a gravitationally driven sink. In problems with large Froude number and strong free-surface deformation, the location of the free surface is not known *a priori*

https://doi.org/10.1017/S0022112010001473 Published online by Cambridge University Press

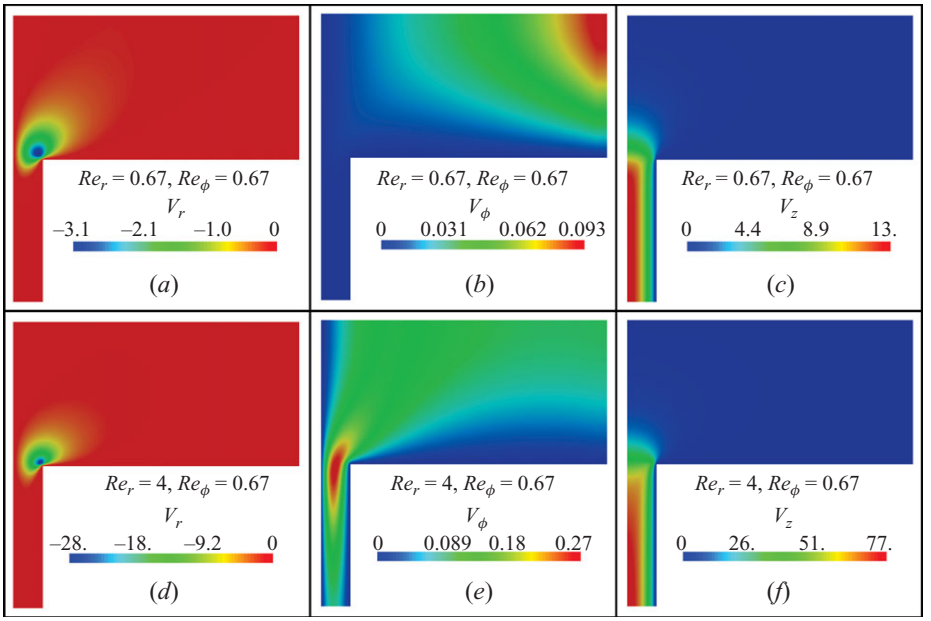


FIGURE 2. Radial, azimuthal and axial velocities for constant azimuthal Reynolds number $Re_\phi = 0.67$ and two different radial Reynolds numbers. (*a–c*) Without a central vortex at $Re_r = 0.67$ and (*d–f*) with a central vortex at $Re_r = 4$.

and it must be obtained as part of the solution as in the simulations by Ito, Sakai & Yamaguchi (2003).

At the inlet, the axial velocity is zero and the radial velocity and the azimuthal velocity are prescribed with the half Poiseuille profiles:

$$V_r = \tfrac{3}{2}\overline{V}_r\,(z/H)(2 - z/H), \quad V_\phi = \tfrac{3}{2}\overline{V}_\phi(z/H)(2 - z/H). \tag{2.5}$$

This choice was made because it matches the boundary conditions at the bottom and at the surface and therefore avoids the development of thin boundary layers at these locations. At the bottom of the drain-pipe, we use an outlet boundary condition similar to that described by Magnaudet *et al.* (1995). Namely, we nullify the second-order normal derivatives of the velocity components as well as the second-order normal-tangential cross-derivatives of the pressure. It was verified that with this choice, the axial velocity profile at the outlet is very close to the Poiseuille law, and that the results are independent of the drain-pipe height, provided that the latter is not too small.

2.3. *Results*

Figure 2 shows velocity components in two cases with $H/R = 0.50$, $R_d/R = 0.10$, $H_d/R = 0.50$ and $Re_\phi = 0.67$. In figure 2(*a–c*), we have $Re_r = 0.67$ and in figure 2(*d–f*) we have $Re_r = 4$. The azimuthal flow structure is qualitatively different in the two situations whereas the meridional flow structure is qualitatively similar despite that the volume flow rates differ by a factor of six. We find a weak overall azimuthal flow at $Re_r = 0.67$ and a central vortex above the drain-hole at $Re_r = 4$. We observe that the value of the azimuthal Reynolds number has little influence on the flow structure, and we find the same scenario in the range $Re_\phi = 0.67$ to $Re_\phi = 6.67$. In the special case in which the azimuthal Reynolds number is zero, there is no vortex flow and

https://doi.org/10.1017/S0022112010001473 Published online by Cambridge University Press

	$R_d/R=0.05$		$R_d/R=0.10$		$R_d/R=0.15$	
H/R	Re_r	Re_d	Re_r	Re_d	Re_r	Re_d
0.25	4.3	2.9	5.3	2.9	6.1	2.9
0.50	2.0	2.7	2.5	2.7	2.9	2.8
0.75	1.5	3.1	1.9	3.1	2.3	3.2

TABLE 1. The radial Reynolds number, Re_r, above which a central vortex is evident decreases with H/R and increases with R_d/R. The corresponding height based radial Reynolds number Re_d has only a weak dependence on H/R and is essentially independent of R_d/R.

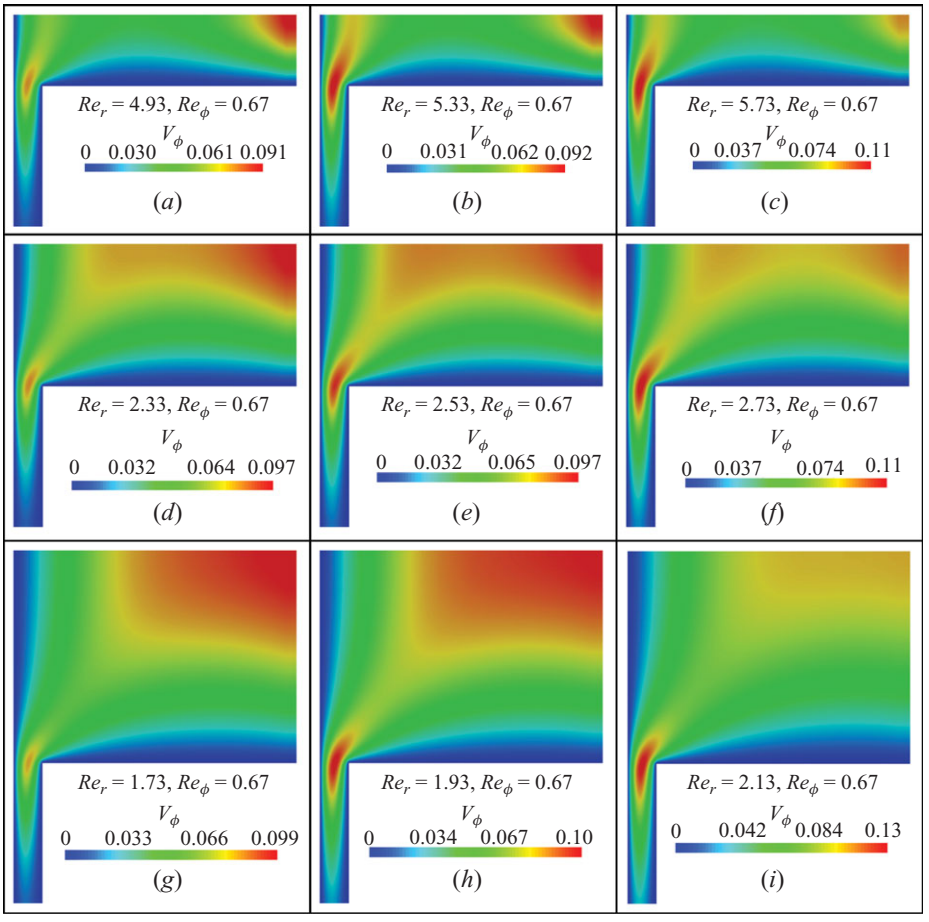


FIGURE 3. Azimuthal velocity for $Re_\phi = 0.67$ and different radial Reynolds numbers for three tanks with different ratio between height and radius. $(a–c)$ With $H/R = 0.25$, $(d–f)$ with $H/R = 0.50$ and $(g–i)$ with $H/R = 0.75$. The fluid has a weak overall rotation in (a, d, g) and a central vortex above the drain-hole is evident in (c, f, i). The intermediate cases (b, e, h) illustrate the transition between the two regimes.

the azimuthal velocity is identically zero everywhere in the tank. For simulations and stability analysis of this state we refer to De Felice (2007).

Figure 3 shows the azimuthal velocity in three different tank geometries. In all three cases we find a weak overall azimuthal flow at a low radial Reynolds number and a central vortex above the drain-hole at a high radial Reynolds number. Table 1

https://doi.org/10.1017/S0022112010001473 Published online by Cambridge University Press

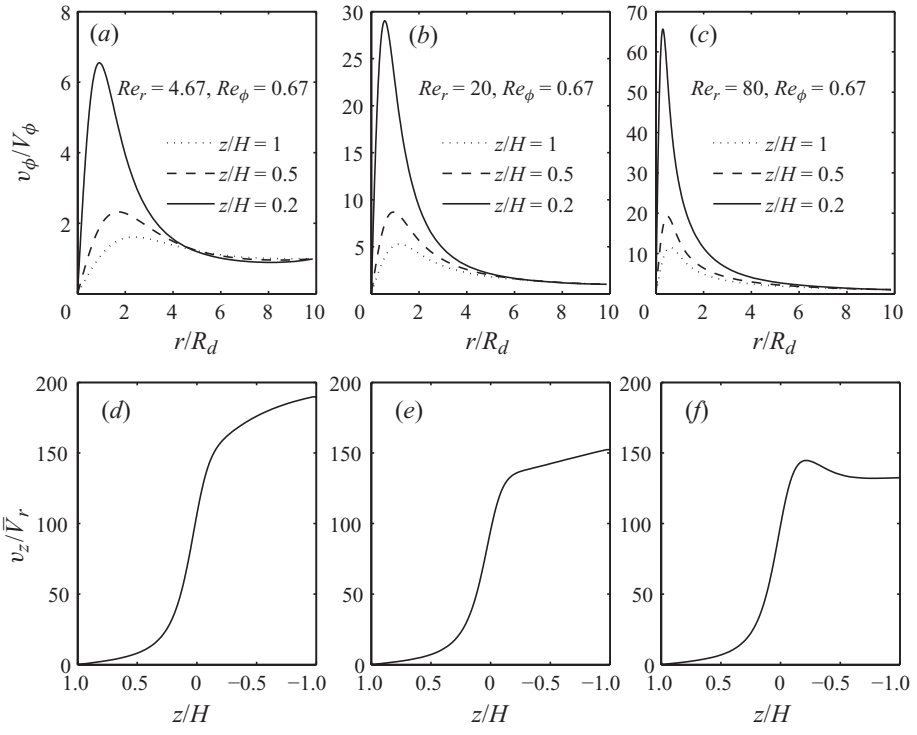


FIGURE 4. Azimuthal and axial velocities on the axis of symmetry for constant azimuthal Reynolds number $Re_\phi = 0.67$ and three different radial Reynolds numbers. (a,d) With $Re_r = 4.67$, (b,e) with $Re_r = 20$ and (c,f) with $Re_r = 80$. The simulations were made with $H/R = 0.50$, $R_d/R = 0.10$ and $H_d/R = 0.50$.

summarizes the parameters for the three cases with $R_d/R = 0.10$ shown in figure 3, three cases with $R_d/R = 0.05$ and three cases with $R_d/R = 0.15$. The value of Re_r above which a central vortex is evident decreases strongly with H/R and increases weakly with R_d/R. We presume that the critical parameter is the strength of the meridional flow immediately above the drain-hole, since the central vortex is most intense in this region. The dependence of the transition on H/R is therefore not surprising, since the average outflow velocity increases with H/R. In agreement with this observation, we find that the value of the height-based radial Reynolds number $Re_d = (H/R)(R_d/R)^{-1/3} Re_r = -(R_d/R)^{-1/3} H \overline{V}_r/\nu$ above which a central vortex is evident is essentially constant as shown in table 1. However, we do not know how to account theoretically for the weak $-1/3$ power law dependence of the transition on R_d/R that is indicated by the simulations.

Figure 4 shows the azimuthal velocity profiles at different heights and the height dependence of the axial down-flow velocity on the axis of symmetry. The radius of the vortex core decreases slowly with radial Reynolds number and increases with height. The maximum of the azimuthal velocity normalized by the azimuthal velocity at the inlet is in the three cases between five and six times larger close above the drain-hole in comparison with the flow at the surface. We notice that the azimuthal velocity normalized by the azimuthal velocity at the inlet in the upper half of the tank has a weak height dependence in comparison with the height dependence in the lower half of the tank. The central down-flow velocity increases linearly downwards

https://doi.org/10.1017/S0022112010001473 Published online by Cambridge University Press

in the upper half of the tank from zero at the surface. Nearer to the drain-hole the height dependence of the central down-flow velocity is not linear and it increases strongly as the drain-hole is approached. The central down-flow velocities normalized by the average radial velocity at the inlet in figure 4(*d–f*) are essentially identical in the upper half of the tank. In the drain-pipe the central down-flow velocity increases downwards in figure 4(*d*) and (*e*), whereas it has a local maximum in figure 4(*f*).

3. Theoretical modelling

We will now investigate a simple theoretical model and compare it with the simulation results for the surface flow. Supported by the simulation results for the flow structure in the upper half of the tank, we shall for simplicity assume that the radial velocity and the azimuthal velocity are both independent of height and that the axial velocity depends linearly on height and vanishes at the surface. The steady solutions of the Navier–Stokes equations with such flow structure were studied systematically by Donaldson & Sullivan (1960) and include the Burgers vortex (Burgers 1940) and the Sullivan two-cell vortex (Sullivan 1959). These solutions are not only exact but also restrictive, and it is hopeless to expect them to match completely with the flow investigated here. Instead, we investigate a class of approximate model solutions where the radial velocity and the axial velocity satisfy the continuity equation (2.1) and where the azimuthal velocity is an exact solution of the azimuthal Navier–Stokes equation (2.3).

3.1. *Einstein and Li model*

The model suggested by Einstein & Li (1951) belongs to the present category and assumes an axial plug-flow restricted to a central down-flow region with radius a. For the axial velocity and the radial velocity we therefore have

$$v_z = \begin{cases} \dfrac{q\,(z-H)}{\pi a^2}, & r < a, \\ 0, & r > a, \end{cases} \qquad v_r = \begin{cases} -\dfrac{q\,r}{2\pi a^2}, & r < a, \\ -\dfrac{q}{2\pi r}, & r > a. \end{cases} \tag{3.1}$$

The azimuthal Navier–Stokes equation (2.3) is solved separately in the two regions, and the matching is done by the requirement that v_ϕ and the shear stress $\sigma_{\phi r}$ are continuous at $r = a$. In general, with $Re_r \neq 2$ we find the solution

$$v_\phi = A \begin{cases} (Re_r - 2)[1 - \mathrm{e}^{-(Re_r/2)(r/a)^2}]\, r^{-1}, & r < a, \\ (Re_r - 2 - 2\,\mathrm{e}^{-Re_r/2}) r^{-1} + Re_r\, \mathrm{e}^{Re_r/2}\, a^{Re_r - 2}\, r^{1-Re_r}, & r > a, \end{cases} \tag{3.2}$$

and for the special case with $Re_r = 2$ we obtain

$$v_\phi = B \begin{cases} \mathrm{e}\,[1 - \mathrm{e}^{-(r/a)^2}]\, r^{-1}, & r < a, \\ [\mathrm{e} - 1 + 2\ln(r/a)]\; r^{-1}, & r > a, \end{cases} \tag{3.3}$$

where the constants A and B are determined by the outer boundary condition $v_\phi = V_\phi$ at $r = R$. The vortex flow in the down-flow region is the Burgers vortex (Burgers 1940) and the two-dimensional flow in the outer region is the exact solution obtained by Hamel (1917) and analysed by Preston (1950) and Thwaites (1950).

3.2. *Integrable model with smooth axial velocity profile*

To construct a more satisfactory description without velocity discontinuities, we introduce a model with concentrated central down-flow and the continuous velocity

https://doi.org/10.1017/S0022112010001473 Published online by Cambridge University Press

profiles:

$$v_z = \frac{q\,a^2(1+(a/R)^2)(z-H)}{\pi(a^2+r^2)^2}, \quad v_r = -\frac{q(1+(a/R)^2)r}{2\,\pi(a^2+r^2)}. \tag{3.4}$$

The meridional flow thus defined is a smooth version of the flow considered by Einstein & Li (1951). In the general case with $Re_r \neq 2/(1+(a/R)^2)$, we insert the radial velocity and integrate the azimuthal Navier–Stokes equation (2.3) to obtain the azimuthal velocity under the remarkably simple form:

$$v_\phi = \frac{C}{r}\left[1-\left(1+\frac{r^2}{a^2}\right)^{1-(Re_r/2)(1+(a/R)^2)}\right], \tag{3.5}$$

and for the special case with $Re_r = 2/(1+(a/R)^2)$ we find

$$v_\phi = \frac{D}{r}\ln\left(1+\frac{r^2}{a^2}\right), \tag{3.6}$$

where the constants C and D are determined by the outer boundary condition $v_\phi = V_\phi$ at $r = R$. The model is only approximate since the solution does not satisfy the radial Navier–Stokes equation (2.2) and the axial Navier–Stokes equation (2.4) in the entire domain. However, the solution satisfies the governing equations evaluated at the surface, and we presume that it is applicable when the ratio of the sink flow to the circulation is small as discussed by Lewellen (1962).

3.3. *Characteristics of the analytical models*

For both approximate models the asymptotic behaviour of the azimuthal velocity at infinity depends qualitatively on the value of the radial Reynolds number. For the smooth model with $Re_r > 2/(1+(a/R)^2)$ it follows that $v_\phi \propto r^{-1}$, which is recognized as the usual inviscid vortex solution. For the smooth model with $Re_r < 2/(1+(a/R)^2)$ we see that $v_\phi \propto r^{1-Re_r(1+(a/R)^2)}$ and that the azimuthal velocity thus decreases less rapidly and that it may even increase if $Re_r < 1/(1+(a/R)^2)$. The radius of the vortex core results from the balance between the outward transport of vorticity due to viscous diffusion and the inward advective transport of vorticity and the axial vortex stretching as discussed in the introduction. In the Einstein and Li model, the radius of the vortex core r_{max}, defined as the location of the maximum of the azimuthal velocity, can be obtained analytically. For $Re_r > 2.5129$, the maximum is located within the plug-flow region and it is given by $r_{max}/a = 1.5852\,Re_r^{-1/2}$. For $1 < Re_r < 2.5129$, the maximum is located outside the plug-flow region and for $Re_r \neq 2$ it is

$$\frac{r_{max}}{a} = \left[\frac{Re_r\,(Re_r-1)}{2+(Re_r-2)\,\mathrm{e}^{Re_r/2}}\right]^{1/(Re_r-2)}. \tag{3.7}$$

For $Re_r < 1$ the azimuthal velocity is an increasing function so that no maximum is reached inside the domain. For the model with the smooth axial velocity profile, the value of r_{max} is not available in analytical form, but it can be obtained numerically. Figure 5(a) shows r_{max}/a as a function of Re_r for both models. At a high radial Reynolds number, the models display the same power law $r_{max}/a \propto Re_r^{-1/2}$. The corresponding value of the maximum of the azimuthal velocity v_{max}/V_ϕ is plotted as a function of Re_r in figure 5(b). Note that both models display the asymptotic behaviour $v_{max}/V_\phi = 0.4513\,(R/a)\,Re_r^{1/2}$ at a high radial Reynolds number.

https://doi.org/10.1017/S0022112010001473 Published online by Cambridge University Press

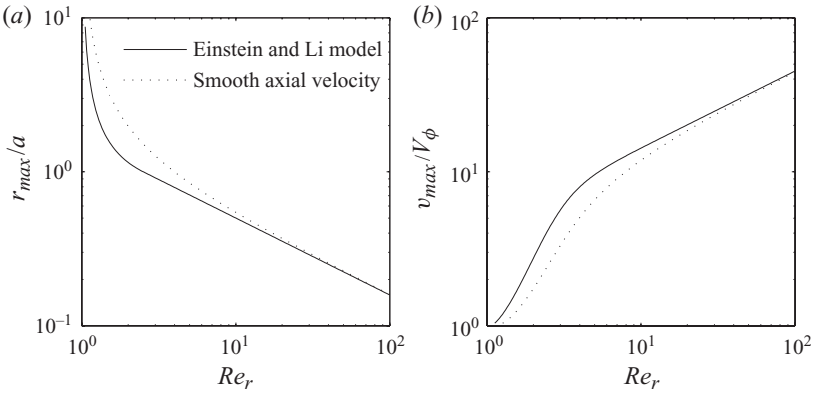


FIGURE 5. The radius of the vortex core (a) and the maximum of the azimuthal velocity (b) as functions of the radial Reynolds number in the two models with $a/R = 0.10$.

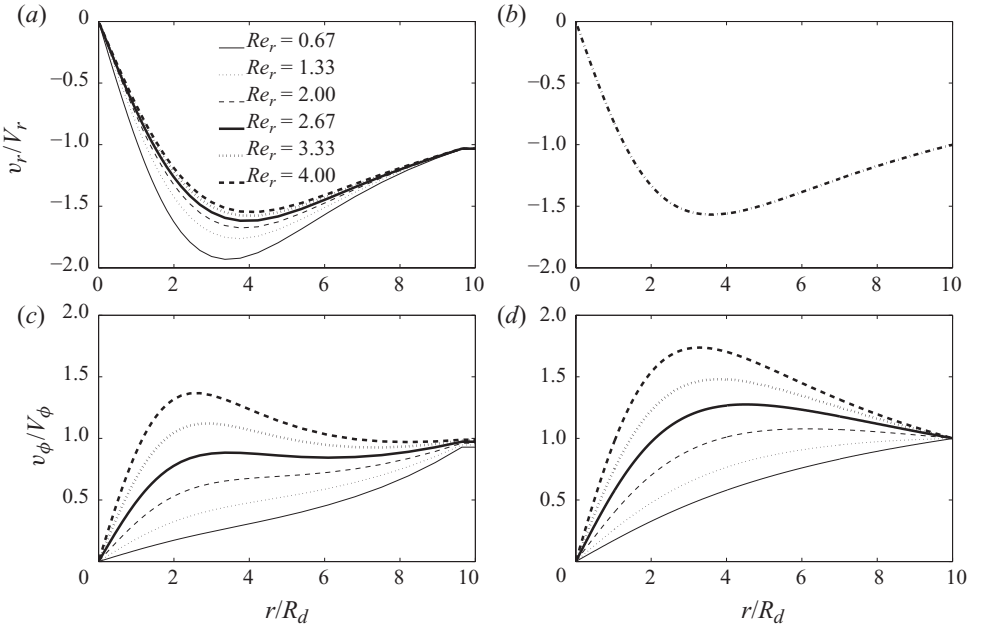


FIGURE 6. Radial and azimuthal velocities at the surface for different radial Reynolds numbers. (a, c) Simulations with $H/R = 0.50$, $R_d/R = 0.10$, $H_d/R = 0.50$ and $Re_\phi = 0.67$. (b, d) Results of the model with smooth axial velocity profile.

3.4. *Simulations versus analytical models*

Figure 6 shows the radial and azimuthal velocities at the surface for different radial Reynolds numbers. The structure of the radial velocity in figure 6(a) is little influenced by the sixfold difference in the volume flow rate and for simplicity we therefore model the radial velocity normalized by the radial velocity at the inlet using the same function in all six cases. The curve in figure 6(b) was obtained by fitting the smooth radial velocity profile (3.4) to the data in this way. The best fit gave $a = 4\,R_d$ for the radius of the average down-flow region. The corresponding azimuthal velocity (3.5) is shown in figure 6(d) and it compares favourably with the simulations

https://doi.org/10.1017/S0022112010001473 Published online by Cambridge University Press

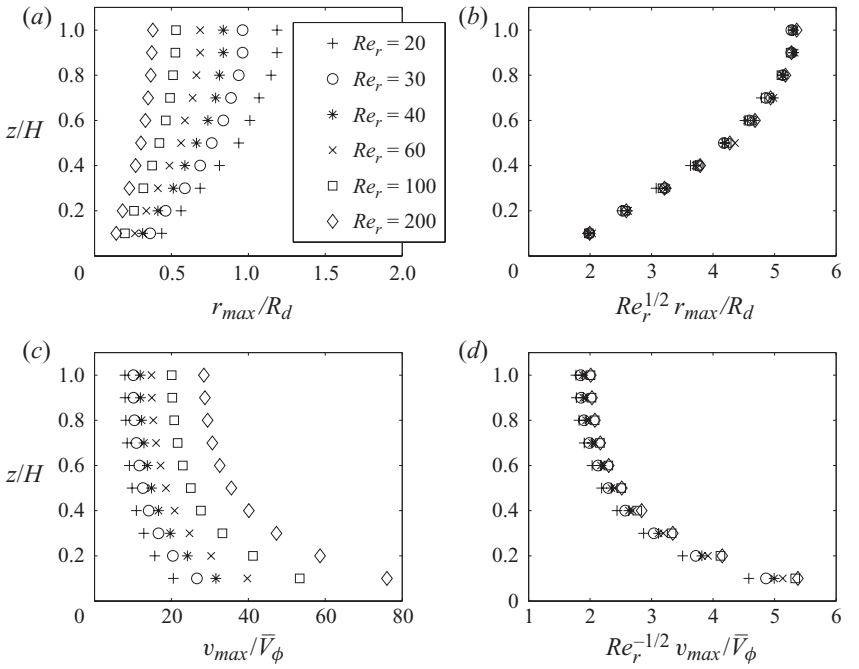


FIGURE 7. (a, b) The radius of the vortex core and (c, d) the maximum azimuthal velocity for different heights and radial Reynolds numbers. The simulations were made with $H/R = 0.50$, $R_d/R = 0.10$, $H_d/R = 0.50$ and $Re_\phi = 0.67$.

in figure 6(c) and has the same qualitative dependence on the radial Reynolds number. The model with the smooth axial velocity profile therefore offers a good description of the surface flow using only the radius of the down-flow region as a free parameter.

It is instructive to compare (3.4) with the flow represented by a point-sink of strength Q at the drain-hole centre at $z = 0$ plus a point-sink of strength Q on the axis of symmetry at $z = 2H$ to ensure that the axial velocity vanishes at the surface (Rott 1958). The point-sink model represents the meridional flow near the drain-hole, but outside the central drain-hole region the flow is more appropriately modelled by a line-sink on the axis of symmetry. At the surface we have $v_r = -Q\, r/(2\pi(H^2 + r^2)^{3/2})$ in the point-sink model, which is analogous to (3.4), but with the power 3/2 in the denominator instead of the power 1. The point-sink model suggests that H is the relevant scale for the radius of the down-flow region at the surface in reasonable agreement with the simulations.

The radius of the vortex core and the maximum of the azimuthal velocity as obtained in the simulations are shown in figure 7 for different heights and radial Reynolds numbers. The radius of the vortex core increases with height as shown in figure 7(a), whereas the maximum of the azimuthal velocity decreases with height as shown in figure 7(c). The vortex is more concentrated and intense at a high radial Reynolds number. We observe that the products $Re_r^{1/2}\, r_{max}$ and $Re_r^{-1/2}\, v_{max}$ collapse on single curves as shown in figure 7(b) and (d), consistent with the asymptotic behaviour predicted by the models and shown in figure 5. We do not know the curves in figure 7(b) and (d) analytically, but we note that the products $r_{max}\, v_{max}$ are approximately height independent and of magnitude $R\, \overline{V}_\phi$.

https://doi.org/10.1017/S0022112010001473 Published online by Cambridge University Press

4. Discussion and outlook

The transition from a weak overall azimuthal flow to a central vortex above the drain-hole is smooth and occurs at radial Reynolds numbers in the range from one to ten. The underlying physical mechanism for the transition is the increase of the inward advective transport of vorticity and the axial vortex stretching. These intensification processes balance the outward viscous diffusion of vorticity. The simple model with the smooth axial velocity profile turned out to describe the surface flow well and to capture the transition. At a high radial Reynolds number, the radius of the vortex core at each given height decreases as one over the square root of the radial Reynolds number and the maximum of the azimuthal velocity at each given height increases as the square root of the radial Reynolds number. This partially describes the vortex intensification. The height dependence of the vortex reflects both the tank geometry and the choice of inlet velocity profiles which give rise to a down-flow region that is more concentrated as the drain-hole is approached. It remains a challenge to model the height dependence of the radius of the vortex core and the maximum of the azimuthal velocity, and it would be interesting if e.g. the boundary layer model of vortex filaments suggested by Rossi *et al.* (2004) could be adapted to model the bathtub vortex.

An experimental realization of a bathtub vortex with control of both the radial and the azimuthal velocities at the inlet was made by Shingubara *et al.* (1988) using a tank with a system of adjustable guide vanes. The fluid layer in the experiment was shallow in comparison with our simulations and different vortex flows were observed experimentally. It would be interesting to explore the bathtub vortex in an experiment using a set-up with the geometry discussed here and a system of adjustable guide vanes. A related and equally interesting problem is vortex formation through spontaneous symmetry breaking in the case where the inlet is designed in order not to introduce any angular momentum. Such experiments are challenging to construct, because even a small misalignment at the inlet can introduce asymmetries that lead to the formation of a central vortex. Our results on the existence conditions of a central vortex provide information to guide the design of such experiments, and we are currently working on this problem.

We thank Benny Lautrup for helpful discussions. We are also thankful to Jørn Christensen and Annaïg Pedrono for valuable computer support.

REFERENCES

Alekseenko, S. V., Kuibin, P. A. & Okulov, V. L. 2007 *Theory of Concentrated Vortices*. Springer.

Andersen, A., Bohr, T., Stenum, B., Juul Rasmussen, J. & Lautrup, B. 2003 Anatomy of a bathtub vortex. *Phys. Rev. Lett.* **91**, 104502.

Auguste, F., Fabre, D. & Magnaudet, J. 2010 Bifurcations in the wake of a thick circular disk. *Theor. Comput. Fluid Dyn.* **24**, 305–313.

Batchelor, G. K. 1967 *An Introduction to Fluid Dynamics*. Cambridge University Press.

Burgers, J. M. 1940 Application of a model system to illustrate some points of the statistical theory of free turbulence. *Proc. Acad. Sci. Amsterdam* **43**, 2–12.

De Felice, V. F. 2007 Il vortice a superficie libera in quanto instabilità. PhD thesis, Università degli Studi di Salerno.

Donaldson, C. duP. & Sullivan, R. D. 1960 Behaviour of solutions of the Navier–Stokes equations for a complete class of three-dimensional viscous vortices. In *Proc. Heat Transfer and Fluid Mech. Institute, Stanford University*, pp. 16–30.

https://doi.org/10.1017/S0022112010001473 Published online by Cambridge University Press

Einstein, H. A. & Li, H. 1951 Steady vortex flow in a real fluid. In *Proc. Heat Transfer and Fluid Mech. Institute, Stanford University*, pp. 33–43.

Guyon, E., Hulin, J. P., Petit, L. & Mitescu, C. D. 2001 *Physical Hydrodynamics*. Oxford University Press.

Hamel, G. 1917 Spiralförmige Bewegungen zäher Flüssigkeiten. *Jahresbericht d. Deutschen Mathem.-Vereinigung* **25**, 34–60.

Ito, K., Sakai, T. & Yamaguchi, A. 2003 Numerical simulation of free surface vortex in cylindrical tank. In *The 10th International Topical Meeting on Nuclear Reactor Thermal Hydraulics (NURETH-10) Seoul, Korea, October 5–9, 2003*, pp. 1–13.

Landau, L. D. & Lifshitz, E. M. 1987 *Fluid Mechanics*, 2nd edn. Butterworth-Heinemann.

Lewellen, W. S. 1962 A solution for three-dimensional vortex flows with strong circulation. *J. Fluid Mech.* **14**, 420–432.

Lugt, H. J. 1995 *Vortex Flow in Nature and Technology*. Krieger.

Magnaudet, J., Rivero, M. & Fabre, J. 1995 Accelerated flows past a rigid sphere or a spherical bubble. Part 1. Steady straining flow. *J. Fluid Mech.* **284**, 97–135.

Miles, J. 1998 A note on the Burgers–Rott vortex with a free surface. *Z. Angew. Math. Phys.* **49**, 162–165.

Preston, J. H. 1950 The steady circulatory flow about a circular cylinder with uniformly distributed suction at the surface. *Aeronaut. Q.* **1**, 319–338.

Rossi, M., Bottausci, F., Maurel, A. & Petitjeans, P. 2004 A Nonuniformly stretched vortex. *Phys. Rev. Lett.* **92**, 054504.

Rott, N. 1958 On the viscous core of a line vortex. *Z. Angew. Math. Phys.* **9**, 543–553.

Shapiro, A. H. 1962 Bath-tub vortex. *Nature* **196**, 1080–1081.

Shingubara, S., Hagiwara, K., Fukushima, R., Kawakubo, T. 1988 Vortices around a sinkhole: phase diagram for one-celled and two-celled vortices. *J. Phys. Soc. Japan* **57**, 88–94.

Stepanyants, Y. A. & Yeoh, G. H. 2008*a* Burgers–Rott vortices with surface tension. *Z. Angew. Math. Phys.* **59**, 1–12.

Stepanyants, Y. A. & Yeoh, G. H. 2008*b* Stationary bathtub vortices and a critical regime of liquid discharge. *J. Fluid Mech.* **604**, 77–98.

Sullivan, R. D. 1959 A two-cell vortex solution of the Navier–Stokes equations. *J. Aerosp. Sci.* **26**, 767–768.

Thwaites, B. 1950 Note on the circulatory flow about a circular cylinder through which the normal velocity is large. *Q. J. Mech. Appl. Math.* **3**, 74–79.

Trefethen, L. M., Bilger, R. W., Fink, P. T., Luxton, R. E., Tanner, R. I. 1965 The bath-tub vortex in the southern hemisphere. *Nature* **207**, 1084–1085.

Tyvand, P. A. & Haugen, K. B. 2005 An impulsive bathtub vortex. *Phys. Fluids* **17**, 062105.

https://doi.org/10.1017/S0022112010001473 Published online by Cambridge University Press